Continuum Mech. Thermodyn. (2010) 22:545–553
DOI 10.1007/s00161-010-0140-2

ORIGINAL ARTICLE

Orlando Avila-Pozos · Gennady Mishuris · Alexander Movchan

Bloch–Floquet waves and localisation within a heterogeneous waveguide with long cracks

Received: 16 February 2010 / Accepted: 3 May 2010 / Published online: 16 June 2010

Abstract A bi-material waveguide is assumed to have an array of sufficiently long cracks parallel to the boundaries. The Bloch–Floquet waves propagating along such a waveguide are dispersive, and the band gaps are clearly identified. Slow waves are supported by a system of long cracks, and such modes are represented by the flat dispersion surfaces. Asymptotic analysis combines a lower-dimensional approximation together with the boundary layers occurring near the crack tips. Stress intensity factors are evaluated via the boundary layer analysis, which is matched with the outer fields corresponding to the lower-dimensional model. Evolution of such an elastic system is discussed as the cracks grow as a consequence of the stress concentration, which occurs for some slow waves leading to the crack opening. The asymptotic analysis is supplied with numerical simulations and physical examples.

Keywords Bloch-Floquet waves · Band gap structure · Asymptotic analysis · Cracks

1 Introduction

Analysis of dispersion properties of Bloch–Floquet waves in cylindrical waveguides has a wide range of applications in physics and mechanics, which includes design of photonic crystal fibres as well as phononic band gap structures for elastic media (see, for example, [1,4–6,9]). Fundamental analysis of dynamic fracture in structured media was developed by Slepyan in his monograph [10]. His ideas incorporated a combination of deep physical knowledge of mechanisms of interaction between elastic waves and elements of microstructured media, as well as elegant mathematical theory leading to functional equations of Wiener–Hopf type for dynamic cracks in lattice structures. Strictly speaking, a crack in a lattice is a very different object compared to a crack in a continuum, and the stresses are not singular near the lattice crack. However, an appropriate boundary layer analysis enables one to see the lattice displacements around the crack tip as a

Communicated by Dr. Stephane Roux.

This article is presented in honour of Professor Leonid Slepyan.

O. Avila-Pozos
Centro de Investigacion en Matemáticas, UAEH, Pachuca, Mexico
E-mail: avilap@uaeh.edu.mx

G. Mishuris (✉)
Institute of Mathematical and Physical Sciences, Wales Institute of Mathematical and Computational Sciences, Aberystwyth University, Aberystwyth, UK
E-mail: ggm@aber.ac.uk

A. Movchan
Department of Mathematical Sciences, University of Liverpool, Liverpool, UK
E-mail: abm@liv.ac.uk

boundary layer corresponding to a crack-like fault in a micro-structured medium. Needless to say, some of the physical phenomena described by Slepyan in [10] for cracks in lattices are non-existent for cracks in continuous media. This includes, for example, a very elegant concept of dissipation of energy via outgoing waves in the elastic lattice generated by the propagating crack. The ideas of Slepyan were followed by many of his students, colleagues and independent researchers in dynamic fracture mechanics. In recent articles [7,8], dynamic cracks were considered in inhomogeneous lattice structures, where inhomogeneity affects the dispersion properties of waves generated by the propagating crack. In particular, for such problems effects of localisation within the lattice containing the crack appear to be important. One of the important features of heterogeneous periodic systems is the presence of band gaps, characterising the range frequencies where propagating modes are not supported, and hence any vibration initiated at a frequency within the band gap will decay exponentially at infinity. However, if a waveguide is damaged, i.e. it contains crack-like defects, the dispersion properties of Bloch–Floquet waves change and the new dispersion diagram will incorporate additional dispersion curves characterised by a small group velocity. In many configurations, the vibration modes, corresponding to slow waves, are localised near the defects. Hence, in elastic structures, such slow waves may lead to the growth of defects and finally to a physical failure of the waveguide.

The asymptotic analysis of a thin waveguide, containing a periodic array of interfacial cracks, was presented in [6]. The lower-dimensional model incorporated a system of vibrating thin beams accompanied by the Bloch–Floquet quasi-periodicity condition. In the same article, the boundary layer analysis was developed to take into account the singular stress at the vertices of cracks. The conditions of exponential decay for the boundary layer yield the junction conditions between the elements of the beam structure in the lower-dimensional model.

Transmission problems for waveguides containing the finite systems of defects (cracks, inclusions or passive mass dampers) were considered in [2]. The corresponding model is reduced to an algebraic system, and the analysis of the transmission matrix enables one to estimate the reflected and the transmitted energies. A special attention is given to slow waves supported by the waveguide with defects.

In this article, we focus on the model of a periodic heterogeneous waveguide with a macro-cell containing several cracks. For the undamaged waveguide, without cracks, the dispersion diagram has band gaps, and the presence of cracks leads to the occurrence of slow waves. The corresponding vibration modes are localised near the cracks. Hence, the transmission properties of a waveguide with cracks differ from that of the undamaged waveguide. We analyse different geometrical configurations of cracks within the macro-cell and discuss evolution of the system of defects along with the dispersion properties of the waveguide.

The structure of this article is as follows. Section 2 gives the governing equations and defines the geometry of the waveguide. The lower-dimensional approximation, involving a system of beams, is discussed in Sect. 3. Section 4 presents the static boundary layer formulation describing the fields near the vertices of the cracks; the same section outlines the structure of the uniform asymptotic approximation of the solution in the waveguide with cracks. Bloch–Floquet waves are discussed in Sect. 5, where we also give the dispersion diagrams and analyse slow waves within the waveguide with cracks. The discussion in Sect. 6 addresses the evolution of the system of defects within the waveguide and the corresponding change of the dispersion properties of Bloch–Floquet waves.

2 Formulation of the problem

Let us consider anti-plane shear vibrations of the waveguide shown in Fig. 1. The structure is assumed to be periodic, with the elementary cell of periodicity consisting of two regions occupied by different elastic materials with shear moduli μ_1, μ_2 and the mass densities ρ_1, ρ_2, with longitudinal cracks of sufficiently large length. We also assume that the cracks do not overlap, and the longitudinal separation between the cracks is sufficiently large.

The displacement field is assumed to be time-harmonic, and hence we shall write the governing equations in terms of amplitude functions.

The algorithm we present in this article is generic, and to simplify the formal description we refer to Fig. 2, which includes two sections corresponding to different materials, and the macro-cell contains two cracks, placed non-symmetrically inside the strip. The left and right sections incorporate the materials with the shear moduli and densities μ_1, ρ_1 and μ_2, ρ_2, respectively. The notations Ω_ε^k, $k = 1, \dots, 8$, are used for thin ligaments around the cracks, as shown in Fig. 2.

The diagram has been deliberately scaled in the vertical direction for clarity of notations. It is assumed that the vertical size is much smaller compared to horizontal parts of the periodic strip.

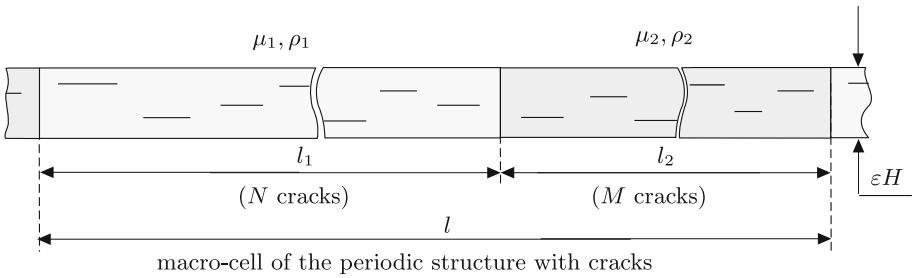

Fig. 1 Heterogeneous periodic waveguide containing cracks.

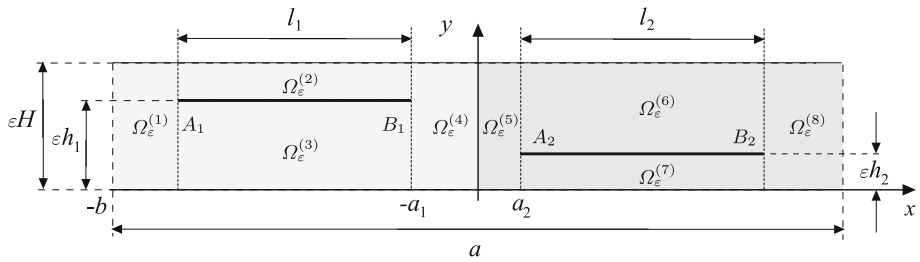

Fig. 2 Geometry of a model of the elementary cell Π_ε of the cracked waveguide

The elementary cell Π_ε is defined by

$$\Pi_\varepsilon = \bigcup_{m=1}^{8} \Omega_\varepsilon^{(m)}$$

Geometrical parameters a, a_1, a_2, l_1, l_2, H and $a - a_1 - a_2 - l_1 - l_2$ are assumed to be of order $O(1)$ whereas $\varepsilon \ll 1$ is a small positive non-dimensional parameter.

The amplitude functions $u_m(x, y)$ are defined in $\Omega_\varepsilon^{(m)}$ as solutions of the Helmholtz equations

$$\Delta u_m(x, y) + \frac{\omega^2}{c_m^2} u_m(x, y) = 0, \quad (x, y) \in \Omega_\varepsilon^{(m)}, \quad m = 1, \ldots, 8, \tag{1}$$

where $c_m = \sqrt{\mu_1/\rho_1}$ for $m = 1, \ldots, 4$, and $c_m = \sqrt{\mu_2/\rho_2}$ for $m = 5, \ldots, 8$, is the shear wave speed in the corresponding part of the heterogeneous waveguide. Conventionally, the quantity ω stands for the radian frequency of the time-harmonic vibrations.

Let M_1 and M_2 be two cracks of the length l_1 and l_2, respectively, defined as follows:

$$M_1 = \{(x, y) : x + a_1 \in (-l_1, 0) \;\; y = \varepsilon h_1\}, \quad M_2 = \{(x, y) : x - a_2 \in (0, l_2) \;\; y = \varepsilon h_2\}.$$

The vertices of the cracks M_p, $p = 1, 2$ are denoted by A_p and B_p (see Fig. 2).

The Neumann boundary conditions are set on the horizontal parts of the boundary of Π_ε

$$\begin{aligned}
\sigma_{yz}(x, \varepsilon H) &:= \mu_1 \frac{\partial u}{\partial y}\Big|_{y=\varepsilon H} = 0, \quad x \in (-b, 0), \\
\sigma_{yz}(x, \varepsilon H) &:= \mu_2 \frac{\partial u}{\partial y}\Big|_{y=\varepsilon H} = 0, \quad x \in (0, a - b), \qquad (2) \\
\sigma_{yz}(x, 0) &:= \mu_1 \frac{\partial u}{\partial y}\Big|_{y=0} = 0, \quad x \in (-b, 0), \\
\sigma_{yz}(x, 0) &:= \mu_2 \frac{\partial u}{\partial y}\Big|_{y=0} = 0, \quad x \in (0, a - b), \qquad (3)
\end{aligned}$$

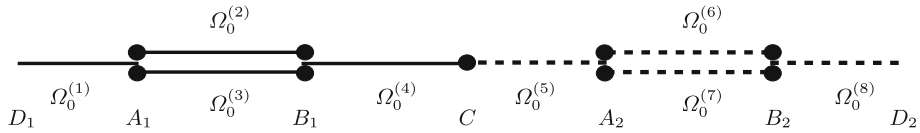

Fig. 3 Skeleton structure of the elementary cell Π_ε

and on the faces of the cracks:

$$\left.\frac{\partial u}{\partial y}\right|_{y=\varepsilon h_1+0} = \left.\frac{\partial u}{\partial y}\right|_{y=\varepsilon h_1-0} = 0, \quad x \in (-l_1 - a_1, -a_1), \tag{4}$$

$$\left.\frac{\partial u}{\partial y}\right|_{y=\varepsilon h_2+0} = \left.\frac{\partial u}{\partial y}\right|_{y=\varepsilon h_2-0} = 0, \quad x \in (a_2, a_2 + l_2). \tag{5}$$

The ideal transmission conditions are set on the interface between $\Omega_\varepsilon^{(4)}$ and $\Omega_\varepsilon^{(5)}$:

$$u(0-, y) = u(0+, y), \quad \mu_1 \frac{\partial u}{\partial x}(0-, y) = \mu_2 \frac{\partial u}{\partial x}(0+, y), \quad y \in (0, \varepsilon H). \tag{6}$$

We seek the solution representing the Bloch–Floquet waves, so that at the ends $x = -b$ and $x = a - b$ we have

$$\begin{aligned} u_1(-b, y) &= e^{-iKa} u_8(a - b, y), \quad y \in (0, \varepsilon H), \\ \tfrac{\mu_1}{\mu_2} \tfrac{\partial}{\partial x} u_1(-b, y) &= e^{-iKa} \tfrac{\partial}{\partial x} u_8(a - b, y), \quad y \in (0, \varepsilon H). \end{aligned} \tag{7}$$

For fixed values of K, it is also assumed that the solution $u = \{u_m\}_{m=1}^8$ has a finite norm in $W_2^1(\Pi_\varepsilon)$, i.e. the finite energy of the eigensolution.

Here and in the text below, we use the notation $u(x, y)$ for eigenfunctions, which are equal to $u_m(x, y)$ in $\Omega_\varepsilon^{(m)}$.

3 Lower-dimensional approximation

Following [6], we use the lower-dimensional model for the leading-order approximation of the displacement amplitude. In the framework of this approach, the macro-cell shown in Fig. 2 is replaced by a skeleton system of "beams", as in Fig. 3. In the following sections we shall also introduce the boundary layers, which serve the junction regions adjacent to the vertices of the cracks.

Here, we outline the governing equations for solution of the one-dimensional model. The notation $\Omega_0^{(m)}$ is used for the limit set corresponding to the thin ligament $\Omega_\varepsilon^{(m)}$. On each one-dimensional segment $\Omega_0^{(m)}$ the function $u_m(x, y)$ is approximated by $v_m(x)$ which solves the equation

$$v_m''(x) + \frac{\omega^2}{c_m^2} v_m(x) = 0 \quad \text{in} \quad \Omega_0^{(m)}, \ m = 1, \dots, 8. \tag{8}$$

The Bloch–Floquet quasi-periodicity conditions are reduced to the form

$$v_8(D_2) = v_1(D_1) e^{iKa}, \quad v_8'(D_2) = \frac{\mu_1}{\mu_2} v_1'(D_1) e^{iKa}. \tag{9}$$

At the point C, corresponding to the interface between the two materials, we have

$$v_4(C) = v_5(C), \quad \mu_1 v_4'(C) = \mu_2 v_5'(C). \tag{10}$$

At the points A_1, B_1 and A_2, B_2 we set the junction conditions. We note that these points correspond to the vertices of cracks, and referring to [6], we remark that these junctions can be understood as conditions of exponential decay of the boundary layers, which occur near the crack vertices. For the current physical configuration, each set of junction conditions represents continuity of the displacements and the overall balance of forces applied to the junction region. We have

$$v_1(A_1) = v_2(A_1) = v_3(A_1), \quad H v_1'(A_1) + (H - h_1) v_2'(A_1) + h_1 v_3'(A_1) = 0, \tag{11}$$

at the junction A_1,

$$v_2(B_1) = v_3(B_1) = v_4(B_1), \quad (H - h_1)v_2'(B_1) + h_1 v_3'(B_1) + H v_4'(B_1) = 0, \tag{12}$$

at the junction B_1,

$$v_5(A_2) = v_6(A_2) = v_7(A_2), \quad H v_5'(A_2) + (H - h_2)v_6'(A_2) + h_2 v_7'(A_2) = 0, \tag{13}$$

at the junction A_2, and

$$v_6(B_2) = v_7(B_2) = v_8(B_2), \quad (H - h_2)v_6'(B_2) + h_2 v_7'(B_2) + H v_8'(B_2) = 0, \tag{14}$$

at the junction B_2. Let us use the notation $\varkappa_m = \omega/c_m$. Then the functions $v_m(x)$, $m = 1, \ldots, 8$, can be represented in the conventional form

$$v_m = \alpha_m \cos(\varkappa_m x) + \beta_m \sin(\varkappa_m x). \tag{15}$$

Direct substitution of (15) into (9)–(14) leads to a system of 16 linear algebraic equations for the constants $\{\alpha_m, \beta_m\}$, $m = 1, \ldots, 8$:

$$\mathfrak{A}(\omega, K)\mathbf{C} = 0, \tag{16}$$

where $\mathbf{C} = \{\alpha_1, \beta_1, \ldots, \alpha_8, \beta_8\}$ and $\mathfrak{A}$ is a matrix function of ω and K. We require

$$\det \mathfrak{A}(\omega, K) = 0, \tag{17}$$

which is the dispersion equation for Bloch–Floquet waves propagating along the periodic structure represented by the skeleton shown in Fig. 3.

The analysis of the system (17) is standard, and we pay a special attention to the standing waves, which may be associated with the cracks existing in the waveguide. Namely, the dispersion diagrams, shown in the further sections, will include flat bands, and for a fixed value of K the eigenmode will correspond to a localised vibration around the crack. The lower-dimensional approximation presented above enables one to estimate the frequency of these waves analytically. The algebraic system with respect to the coefficients $\{\alpha_m, \beta_m\}$ has two classes of obvious non-trivial solutions. The first class of the solutions corresponds to the standing waves around the cracked regions (those vibration modes correspond to the "thin beam" with fixed ends). Namely, if the beams above or below the crack have the length l_j, $(j = 1, 2)$ and are characterised by the material constants μ_j, ρ_j, then the lowest frequency of the standing wave is given by

$$\omega_*^{(j)} = \pi l_j^{-1} \sqrt{\mu_j/\rho_j}. \tag{18}$$

Whilst the ligaments above and below the crack vibrate with the same frequency, their amplitudes of vibration may be different for the cases when the crack is offset from the axis of the waveguide. Namely, the functions v_m are approximated in the form

$$v_m = \mathcal{A}_m \sin(\pi x/l_j), \quad \text{with } j = 1 \text{ for } m = 1, 2, 3, 4 \text{ and } j = 2 \text{ otherwise}, \tag{19}$$

where the constants $\mathcal{A}_m$ satisfy the relations:

$$(H - h_1)\mathcal{A}_2 + h_1\mathcal{A}_3 = 0 \quad \text{and} \quad (H - h_2)\mathcal{A}_6 + h_2\mathcal{A}_7 = 0. \tag{20}$$

The second class of the solutions corresponds to the waveguide without cracks.

Although the above algebraic procedure has been described for the macro-cell with two cracks, the generic algorithm is extendable to a larger array of N-cracks as shown in Fig. 1. The algebraic system incorporating the junction conditions near the crack ends, together with the interface contact conditions, are similar to (11)–(14).

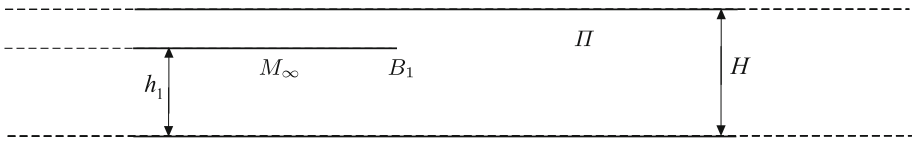

Fig. 4 Boundary layer Π near the crack tip B_1

4 Boundary layer

The boundary layers in the vicinity of the vertices of cracks are represented by solutions of the model problems in the infinite strip Π containing a semi-infinite crack M_∞, as shown in Fig. 4. Since solutions of boundary layer problems near the points A_j, B_j, $j = 1, 2$ have a similar structure, we highlight the features of the problem corresponding to the point B_1, and refer for further details to the article [6].

The scaled variables ξ, η are introduced as follows

$$\xi = \varepsilon^{-1}(x + a_1), \quad \eta = \varepsilon^{-1} y. \tag{21}$$

The notation $W(\xi, \eta)$ is used for the boundary layer, which satisfies the boundary value problem

$$\Delta_{\xi\eta} W(\xi, \eta) = F(\xi, \eta), \quad (\xi, \eta) \in \Pi, \tag{22}$$

together with the conditions at the boundaries

$$\frac{\partial W}{\partial \eta} = 0 \quad \text{on} \quad \partial\Pi \text{ and } \partial M, \tag{23}$$

and the conditions of exponential decay at infinity

$$W(\xi, \eta) = O(\exp(-\gamma|\xi|)), \quad \xi \to \pm\infty, \tag{24}$$

where γ is a positive constant. The right-hand side F in the Eq. 22 is the self-balanced discrepancy brought by the "outer approximation" obtain from the lower-dimensional model, whereas the solvability in the class of exponentially vanishing functions is ensured by the junction conditions (12) at the point B_1. Other junction conditions listed above guarantee exponential decay of boundary layers near the vertices A_1, A_2 and B_2.

The boundary layer is characterised by the following asymptotic representation near the vertex of the crack

$$W(\xi, \eta) \sim \frac{2\mathcal{K}}{\mu}\sqrt{\mathcal{R}}\sin(\theta/2), \quad \text{as } \mathcal{R}^2 = \xi^2 + \eta^2 \to 0, \tag{25}$$

and the coefficient $\mathcal{K}$, referred to as the stress intensity factor, is evaluated in terms of the derivatives of the outer solution as follows

$$\mathcal{K} = \frac{\mu}{2\pi}\sqrt{\frac{(H - h_1)h_1}{H}}|v_2'(B_1) - v_3'(B_1)|. \tag{26}$$

This implies that the stress intensity factor, to leading order, is proportional to the "crack opening", and hence those vibration modes accompanied by the opening of cracks may lead to fracture, the growth of cracks. In Sect. 5, we analyse the dispersion diagrams.

5 Dispersion of Bloch–Floquet waves and localisation near cracks

In this section, we make use of the asymptotic approach, outlined above, and discuss the dispersion properties of waves propagating along the waveguide with cracks. In particular, we pay attention to the occurrence of standing waves, whose amplitude functions are negligibly small outside neighbourhoods of the cracks, whereas in the vicinity of cracks they show a non-zero "crack opening".

The dispersion Eq. 17 has been solved numerically, and the corresponding dispersion diagram, which shows ω as a function of the Bloch parameter K, is presented in Fig. 5a. For this computational example we have used titan (material 1) and aluminium (material 2), and accordingly the material parameters were chosen as follows: $\mu_1 = 4.14 \times 10^{10}$[N m^{-2}], $\mu_2 = 2.6 \times 10^{10}$[N m^{-2}], $\rho_1 = 4420$[kg m^{-3}], $\rho_2 = 2700$[kg m^{-3}]. It

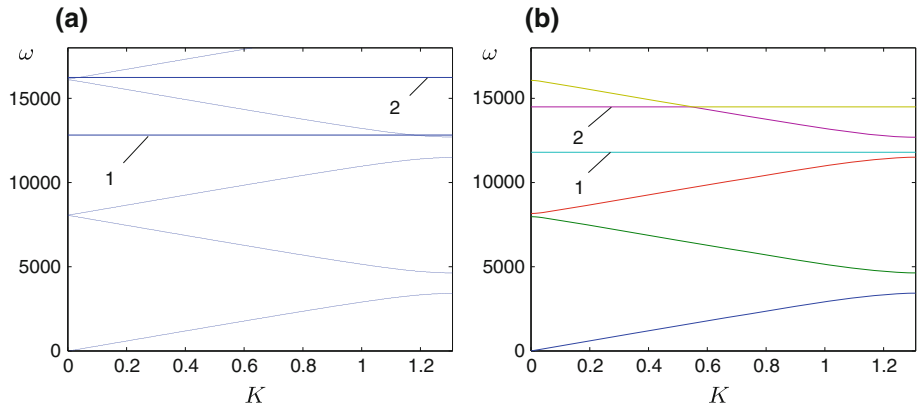

Fig. 5 Dispersion diagrams: (**a**) asymptotic approximation based on the one-dimensional skeleton model and (**b**) COMSOL computation for the two-dimensional macro-cell with cracks. The physical parameters, used in the computation, are $\mu_1 = 4.14 \times 10^{10}[N\ m^{-2}]$, $\mu_2 = 2.6 \times 10^{10}[N\ m^{-2}]$, $\rho_1 = 4420[kg\ m^{-3}]$, $\rho_2 = 2700[kg\ m^{-3}]$. The geometrical parameters are $a = 2.4[m]$, $d = a/2$, $l_1 = 0.75[m]$, $l_2 = 0.6[m]$, $\varepsilon H = 0.2[m]$, $\varepsilon h_1 = 0.1[m]$, and $\varepsilon h_1 = 0.07[m]$

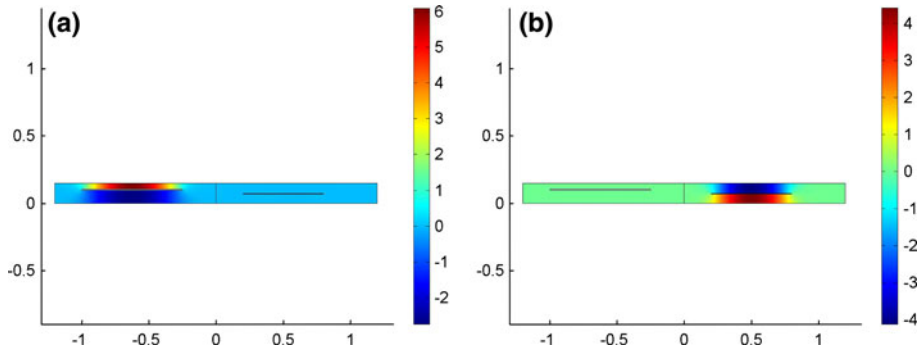

Fig. 6 COMSOL computation of standing wave modes for the waveguide with cracks: (**a**) the first standing mode corresponding to the radian frequency ω_1, (**b**) the second standing mode ω_2 corresponding to ω_2

is also noted that the shear wave speeds of these materials are fairly close to each other: $c_1 = 3060.5[\text{m}\ \ \text{s}^{-1}]$ and $c_2 = 3103.2[\text{m}\ \ \text{s}^{-1}]$. The geometrical parameters are chosen to be $a = 2.4[\text{m}]$, $d = a/2$, $l_1 = 0.75[\text{m}]$, $l_2 = 0.6[\text{m}]$, $\varepsilon H = 0.2[\text{m}]$, $\varepsilon h_1 = 0.1[\text{m}]$ and $\varepsilon h_2 = 0.07[\text{m}]$.

Alongside these computations, Fig. 5b presents the dispersion diagram based on the results of finite element computations in COMSOL performed for the two-dimensional spectral problem formulated in Sect. 2. These two diagrams show a remarkable agreement between the asymptotic lower-dimensional approximation and the independent finite element computations of the full two-dimensional model. For the current choice of geometrical and physical parameters, the discrepancy between the asymptotic approximation (18) of frequencies of standing waves and the accurate numerical results does not exceed 10%, whereas the dispersion curves corresponding to non-zero group velocities in Fig. 5a and b are visually indistinguishable. The frequencies of two standing waves shown in Fig. 5 are $\omega_1 = 11796[\text{Hz}]$, $\omega_2 = 14494[\text{Hz}]$ for the COMSOL and $\omega_1 = 12820[\text{Hz}]$, $\omega_2 = 16240[\text{Hz}]$ for the asymptotic approximation based on the one-dimensional skeleton model. As follows from the analytical lower-dimensional model of Sect. 3, the dispersion diagram consists of the curves, which are very close to that of the waveguide without cracks, and additionally we have slow waves represented by flat bands, where the corresponding vibration modes are localised near the cracks.

In the COMSOL computation, the standing waves, corresponding to the modes 1 and 2 on the dispersion diagram in Fig. 5b, are represented by the displacement fields shown in Fig. 6. It is clearly visible that the displacements are negligibly small outside neighbourhoods of the cracks, whereas the crack faces oscillate, so that the stress intensity factors defined according to (26) are non-zero. Thus, such standing waves may lead to fracture and further elongation of cracks.

We also note that the set of parameters used in the current computation defines the waveguide, characterised by the finite width band gaps clearly visible on the dispersion diagram Fig. 5b. Within the range of frequencies corresponding to these band gaps, no Bloch–Floquet modes are allowed for a waveguide without cracks. On

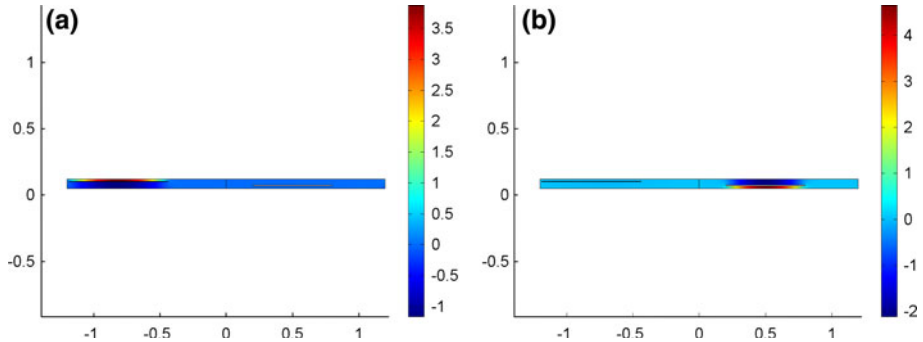

Fig. 7 COMSOL computation for standing waves within a thin strip with cracks: (**a**) first standing mode corresponding to the frequency $\omega_1 = 12333[Hz]$, (**b**) second standing mode corresponding to the frequency $\omega_2 = 15429[Hz]$

the contrary, when crack-like defects are introduced into the elementary cell we observe slow waves attributed to the vibration of the crack faces. On the dispersion diagram, the corresponding dispersion curves of very low group velocity may be imbedded into the band gap intervals evaluated earlier for the case of the undamaged waveguide. Exactly this situation has been implemented in Fig. 6b, where a dispersion curve corresponding to the slow wave runs inside the second band gap. Hence, this significantly changes the filtering properties of the structured waveguide.

Needless to say, the accuracy of the asymptotic approximation based on the lower-dimensional skeleton model of Sect. 3 improves when we decrease ε, i.e. decrease the thickness of the waveguide. As an illustration, we include Figs. 7 and 8 associated with a sufficiently thin waveguide containing cracks. The materials are chosen to be the same as in Fig. 6, whereas the geometrical parameters have changed. Namely, we have $a = 2.4$[m], $d = a/2$, $l_1 = 0.75$[m], $l_2 = 0.6$[m], $\varepsilon H = 0.07$[m], $\varepsilon h_1 = 0.05$[m] and $\varepsilon h_2 = 0.02$[m]. For this case, the first two standing waves have the following frequencies: $\omega_1 = 12333$[Hz], $\omega_2 = 15429$[Hz] for the COMSOL finite element computation, and $\omega_1 = 12820$[Hz], $\omega_2 = 16248$[Hz] for the asymptotic approximations based on the lower-dimensional skeleton model.

6 Discussion

The asymptotic model presented above, accompanied by the COMSOL simulations, delivers a simple algorithm for analysis of damage of structured waveguides. Numerical simulations show that the derivatives of displacements corresponding to standing waves concentrated around cracks are discontinuous near the crack vertices, and the stress components are singular. According to (26) the stress intensity factor is proportional to the crack opening obtained from the lower-dimensional model for the standing waves. In turn, the crack may grow and hence this would lower the frequency of the corresponding standing wave. The bulk of energy is carried by the low frequency waves, and the presence of a low frequency vibration mode with discontinuous displacement will lead to further fracture and delamination of the waveguide.

If the vertices of cracks are sufficiently distant from the interface between two materials, then according to (19), (26), the stress intensity factors at both vertices of the crack are equal, as from the asymptotic approximation based on the lower-dimensional skeleton approximation. On the contrary, when one of the crack vertices approaches the interface, the boundary layer construction of Sect. 4 is not valid any longer, and the stress intensity factors are no longer equal at different vertices of the crack. In this case, new asymptotic formulae for the stress intensity factors have to be used, and the skeleton model of Sect. 3 would require modification. This conclusion is also confirmed by the direct finite element simulations in COMSOL. We also note that in contrary to the values of the stress intensity factors, the dispersion diagrams are less sensitive to the longitudinal shift of the crack within the same phase of the bi-material macro-cell.

Finally, we emphasise that the asymptotic model used here refers to solutions of boundary value problems in thin domains, i.e. the thickness of each ligament $\Omega_\varepsilon^{(m)}$ within the elementary cell is smaller compared to its length. Indeed, as illustrated in the text, the computational model is easily extendable to the situation when the cracks become close to the interface boundary, but the asymptotic approximation would require an additional boundary layer describing a semi-infinite crack near the interface. Although this would considerably change the pointwise approximation of the solutions within the elementary cell, it has been shown that the dispersion

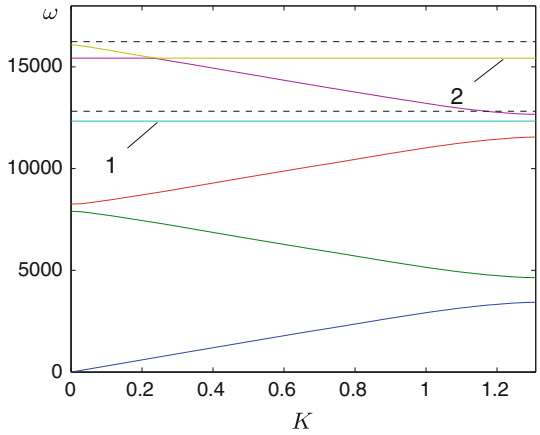

Fig. 8 Dispersion diagrams obtained in COMSOL for a thin strip containing long cracks. The dashed lines correspond the asymptotic approximations of the frequencies of the standing waves obtained from the lower-dimensional skeleton model

properties of the low frequency Bloch–Floquet waves are still well predicted by the asymptotic model (see Figs. 7 and 8). Stress intensity factors are usually considered as important characteristics of the fracture models. They are not essential though in the present case concerned with the evaluation of the dispersion properties of Bloch–Floquet waves. Formula (26) is included specifically to emphasise the link between the "outer solution", away from the crack tip, and the inner solution, which is valid in the immediate neighbourhood of the vertex of the crack. In addition, we note that the advance of fracture and consequently its stability or otherwise can be addressed for the dynamic response of the cracked waveguide; however, this task lies beyond the scope of this article.

The computational examples are given for the case when the elementary cell has only two cracks. This does not change the level of generality of the model and the general idea extends for the case of a finite number of cracks within the elementary cell subject to the constraint that all ligaments $\Omega_\varepsilon^{(m)}$ are thin. Needless to say, the algorithm is extendable to the vector case of the two-dimensional Navier system; flexural vibrations of ligaments may be important in this situation—this would also change the nature of boundary layers and the junction conditions.

References

1. Bigoni, D., Gei, M., Movchan, A.: Dynamics of a prestressed stiff layer on an elastic half space: filtering and band gap characteristics of periodic structural models derived from long-wave asymptotics. J. Mech. Phys. Solids **56**(7), 2494–2520 (2008)
2. Brun M, Movchan A, Movchan N.: Shear polarisation of elastic waves by a structured interface. Continuum Mech. Thermodyn. (2010, submitted)
3. Brun M, Guenneau S, Movchan A, Bigoni D.: Dynamics of structural interfaces: filtering and ficussing effects for elastic waves. J. Mech. Phys. Solids (2010, submitted)
4. Gei, M., Movchan, A., Bigoni, D.: Band-gap shift and defect-induced annihilation in prestressed elastic structures. J. Appl. Phys. **105**(6), 063507 (2009)
5. Linton, C.M., McIver, M.: Periodic structures in waveguides. Proc. R. Soc. A **458**, 3003–3021 (2002)
6. Mishuris, G., Movchan, A., Bercial, J.: Asymptotic analysis of Bloch–Floquet waves in a thin bi-material strip with a periodic array of finite-length cracks. Waves Random Complex Media **17**(4), 511–533 (2007)
7. Mishuris, G., Movchan, A., Slepyan, L.: Waves and fracture in an inhomogeneous lattice structure. Waves Random Complex Media **17**(4), 409–428 (2007)
8. Mishuris, G., Movchan, A., Slepyan, L.: Dynamics of a bridged crack in a discrete lattice. Q. J. Mech. Appl. Math. **61**(2), 151–160 (2008)
9. Movchan, A., Movchan, N., McPhedran, R.: Bloch–Floquet bending waves in perforated thin plates. Proc. R. Soc. A **463**, 2505–2518 (2007)
10. Slepyan, L.: Models and Phenomena in Fracture Mechanics. Springer, Berlin (2002)